ACES Asian Chemical Editorial Society
DOI: 10.1002/asia.201501329
CHEMISTRY AN ASIAN JOURNAL Focus Review

Water Oxidation

SPECIAL ISSUE

Homogeneous and Heterogeneous Photocatalytic Water Oxidation by Persulfate

Shunichi Fukuzumi,*[a, b, c] Jieun Jung,[a] Yusuke Yamada,*[d] Takahiko Kojima,*[e] and Wonwoo Nam*[a]

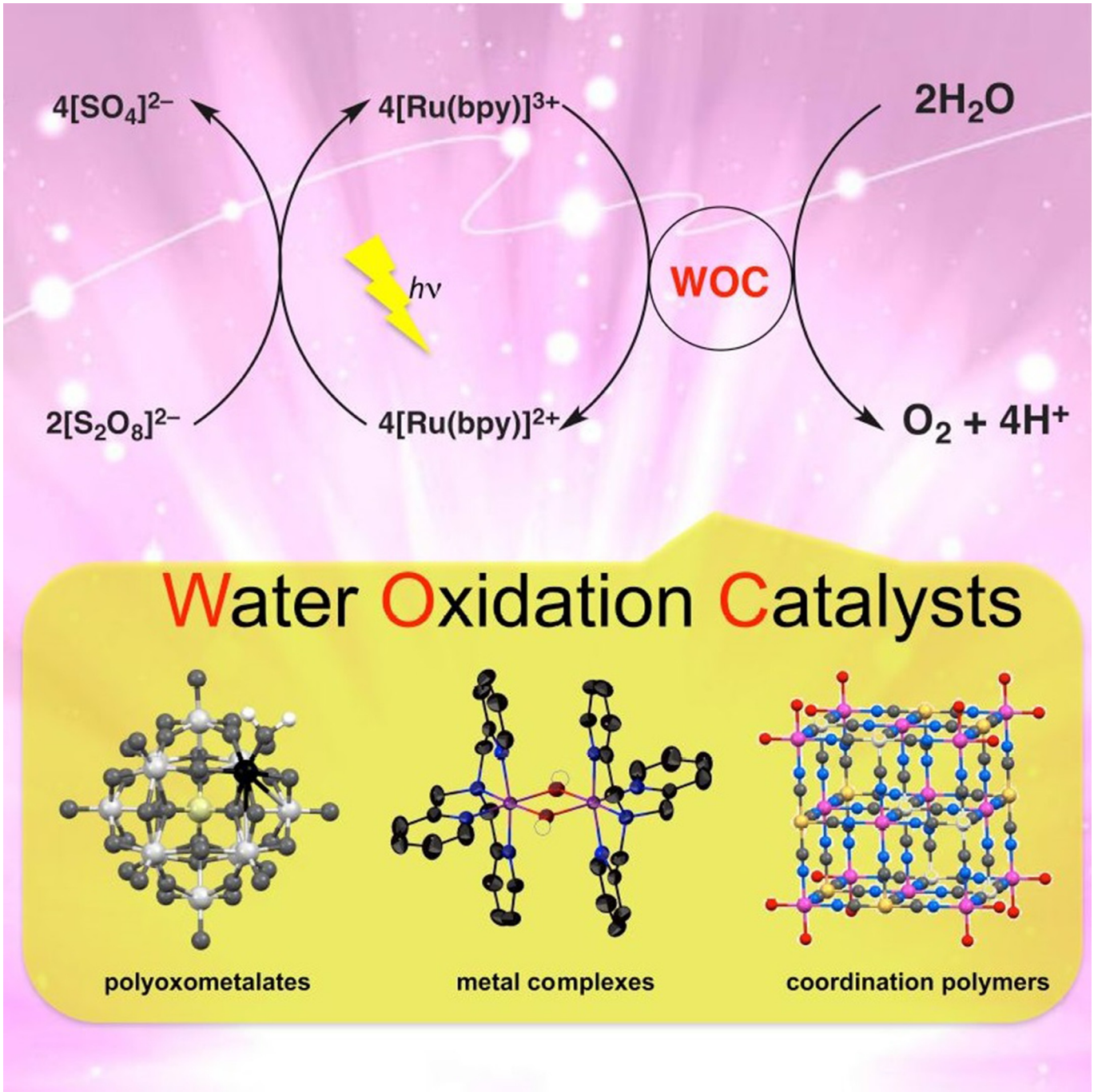

Abstract: Photocatalytic water oxidation by persulfate ($Na_2S_2O_8$) with $[Ru(bpy)_3]^{2+}$ (bpy = 2,2′-bipyridine) as a photocatalyst provides a standard protocol to study the catalytic reactivity of water oxidation catalysts. The yield of evolved oxygen per persulfate is regarded as a good index for the catalytic reactivity because the oxidation of bpy of $[Ru(bpy)_3]^{2+}$ and organic ligands of catalysts competes with the catalytic water oxidation. A variety of metal complexes act as catalysts in the photocatalytic water oxidation by persulfate with $[Ru(bpy)_3]^{2+}$ as a photocatalyst. Herein, the catalytic mechanisms are discussed for homogeneous water oxidation catalysis. Some metal complexes are converted to metal oxide or hydroxide nanoparticles during the photocatalytic water oxidation by persulfate, acting as precursors for the actual catalysts. The catalytic reactivity of various metal oxides is compared based on the yield of evolved oxygen and turnover frequency. A heteropolynuclear cyanide complex is the best catalyst reported so far for the photocatalytic water oxidation by persulfate and $[Ru(bpy)_3]^{2+}$, affording 100% yield of O_2 per persulfate.

1. Introduction

One of the most important challenges that we are facing in the 21st century is definitely the development of artificial photosynthesis to provide a sustainable energy supply using solar energy.[1–23] Photosynthesis is the process to take four electrons and four protons from water, which requires solar energy.[24–27] A deeper understanding of the structure and function of the 'natural' photosynthetic process provides a source of insight and inspiration for discovering how solar energy can be stored in a chemical bond as a low-mass, high-energy carrier fuel.[4–23] Artificial photosynthesis consists of several processes composed of light-harvesting, charge-separation, and water oxidation and reduction processes, mimicking natural photosynthesis.[4–23] The most challenging part among those processes is to develop efficient catalysts for water oxidation like the oxygen-evolving complex (OEC) in photosystem II.[28–38]

$[Ru(bpy)_3]^{3+}$ (bpy = 2,2′-bipyridine) has been frequently used as an oxidant for water oxidation to study the catalytic reactivity, including photodriven catalytic water oxidation because of its ability to react as a pure one-electron oxidant, the wide range of reduction potentials accessible through ring substitution, pH-independent potentials, high quantum yield of photogeneration, and characteristic absorption spectra of both $[Ru(bpy)_3]^{3+}$ and $[Ru(bpy)_3]^{2+}$, which allow the water oxidation reaction to be easily monitored by using a UV/Vis spectrophotometer.[39,40] Production of $[Ru(bpy)_3]^{3+}$ in high quantum and chemical yields can be readily achieved through the oxidative quenching of the excited state of $[Ru(bpy)_3]^{2+}$ by persulfate ($S_2O_8^{2-}$) in an aqueous solution (Scheme 1). The $SO_4^{\bullet-}$ radical anion produced by dissociative electron transfer from $[Ru(bpy)_3]^{2+*}$ to $S_2O_8^{2-}$ can oxidize another equivalent of $[Ru(bpy)_3]^{2+}$ to $[Ru(bpy)_3]^{3+}$. Since water can be oxidized by $[Ru(bpy)_3]^{3+}$ in the presence of water oxidation catalysts, the photocatalytic water oxidation with persulfate provides a standard protocol to study the catalytic reactivity of water oxidation catalysts.

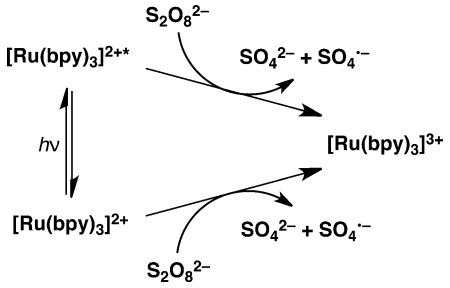

Scheme 1. Oxidative quenching of the excited state of $[Ru(bpy)_3]^{2+}$ by $S_2O_8^{2-}$.

The scope of the current review is to comprehensively compare the catalytic reactivity of water oxidation catalysts in the photocatalytic water oxidation by persulfate using $[Ru(bpy)_3]^{2+}$ as a photocatalyst. First, the catalytic reactivities and mechanisms of metal complexes acting as homogeneous catalysts in water oxidation reactions are compared and discussed. Then,

[a] *Prof. Dr. S. Fukuzumi, Dr. J. Jung, Prof. Dr. W. Nam*
Department of Chemistry and Nano Science
Ewha Womans University
Seoul 120-750 (Korea)
E-mail: fukuzumi@chem.eng.osaka-u.ac.jp
wwnam@ewha.ac.kr

[b] *Prof. Dr. S. Fukuzumi*
Faculty of Science and Engineering
Meijo University
ALCA and SENTAN
Japan Science and Technology Agency (JST)
Nagoya, Aichi 468-0073 (Japan)

[c] *Prof. Dr. S. Fukuzumi*
Graduate School of Engineering
Osaka University
ALCA and SENTAN
Japan Science and Technology Agency (JST)
Suita, Osaka, 565-0871 (Japan)

[d] *Prof. Dr. Y. Yamada*
Department of Applied Chemistry and Bioengineering
Graduate School of Engineering
Osaka City University
3-3-138 Sugimoto, Sumiyoshi, Osaka 558-8585 (Japan)
E-mail: ymd@a-chem.eng.osaka-cu.ac.jp

[e] *Prof. Dr. T. Kojima*
Department of Chemistry, Faculty of Pure and Applied Science
University of Tsukuba
1-1-1 Tennoudai, Tsukuba, Ibaraki 305-8571 (Japan)
E-mail: kojima@chem.tsukuba.ac.jp

This manuscript is part of a special issue on energy conversion and storage. Click here to see the Table of Contents of the special issue.

the conversion of homogeneous catalysts to metal oxide nanoparticles during the water oxidation is discussed to clarify the actual heterogeneous catalysts produced from the precursor metal complexes in homogeneous solution. Finally, the catalytic activity of various metal oxide nanoparticles is compared in the $[Ru(bpy)_3]^{2+}$-photocatalyzed water oxidation by persulfate to develop the most efficient water oxidation catalyst affording 100% yield of O_2.

2. Homogeneous Catalysts

Extensive efforts have been devoted to develop homogeneous water oxidation catalysts (WOCs) in the photocatalytic water oxidation by persulfate as an oxidant with $[Ru(bpy)_3]^{2+}$ as a photocatalyst.[41–66] The turnover numbers (TONs) and the yields of O_2 are summarized in Table 1. Molecular polyoxometalates (POMs) have been developed as efficient WOCs because inorganic ligands of POMs are hardly oxidized during the water oxidation.[67–69] An iron-based POM, $[Fe_{11}(H_2O)_{14}(OH)_2(W_3O_{10})_2(\alpha\text{-}SbW_9O_{33})_6]^{27-}$, acts as the most efficient catalyst in the $[Ru(bpy)_3]^{2+}$-photocatalyzed water oxidation by persulfate, affording a high TON (1815) and a high O_2 yield per persulfate (94%) at pH 10 in a sodium borate buffer aqueous solution.[41] The O_2 yield is defined as twice the number of moles of O_2 per mole of $Na_2S_2O_8$ because two moles of $Na_2S_2O_8$ are required for the four-electron oxidation of H_2O to evolve O_2. The catalytic cycle of visible-light-driven water oxidation by persulfate and $[Ru(bpy)_3]^{2+}$ is shown in Scheme 2. $[Ru(bpy)_3]^{3+}$ produced by oxidative electron-transfer quenching of $[Ru(bpy)]^{2+*}$ by persulfate (Scheme 1) can oxidize water by the catalysis of a WOC (Scheme 2).

The initial reaction rate of 7.9 mmol min^{-1} (the oxygen evolution rate in the first 60 s of light illumination) and $TOF_{initial}$ (TON 1 min/60 s) of 6.3 s^{-1} in the photocatalytic oxidation with the Fe-POM are the largest among the data in Table 1.[41] The

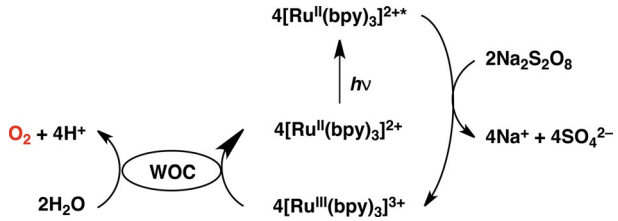

Scheme 2. Photocatalytic cycle for water oxidation by persulfate with $[Ru(bpy)_3]^{2+}$ and WOC.

Shunichi Fukuzumi earned a bachelor's degree and PhD degree in applied chemistry at Tokyo Institute of Technology in 1973 and 1978, respectively. After working as a postdoctoral fellow (1978–1981) at Indiana University in USA, he joined the Department of Applied Chemistry, Osaka University, as an Assistant Professor in 1981 and was promoted to a Full Professor in 1994. His research interests are artificial photosynthesis and electron transfer chemistry. He is now a Distinguished Professor of Ewha Womans University, a Designated Professor of Meijo University, a Professor Emeritus of Osaka University, and the leader of an ALCA (Advanced Low Carbon Technology Research and Development) project that started in 2011.

Jieun Jung earned a bachelor's degree from Chungnam National University, Korea in 2010, and PhD degree from Osaka University, Japan in 2015. She is now working as a postdoctoral fellow at Ewha Womans University.

Yusuke Yamada earned his PhD degree in macromolecular science from Osaka University in 1998. He was working as a researcher and senior researcher at Osaka National Research Institute (currently AIST) from 1998 to 2009. From 2007 to 2008, he was a visiting scholar at UC Berkeley. He was an associate professor of Osaka University from 2009. In 2015, he moved to Osaka City University as a Professor.

Takahiko Kojima is a Professor of the Department of Chemistry at University of Tsukuba. He received his BE (1986) and PhD (1991) from the University of Tokyo. After post-doctoral work at University of Minnesota, USA, he became a Research Associate at the Department of Chemistry at Kyushu University in Japan in 1994, and then moved to Osaka University as an Associate Professor in 2005. In 2008, he moved to Tsukuba. His research interest involves bioinspired redox chemistry of ruthenium complexes and development of functional π-space based on non-planar π-systems.

Wonwoo Nam received his BS (Honors) degree in Chemistry at California State University, Los Angeles (1985), and his PhD degree in Inorganic Chemistry at UCLA (1990). After one year postdoctoral experience at UCLA, he became an Assistant Professor at Hong Ik University in 1991. He moved to Ewha Womans University in 1994, where he is presently a Distinguished Professor of Ewha Womans University. His current research focuses on the dioxygen activation, water oxidation, and sensors for metal ions in bioinorganic chemistry.

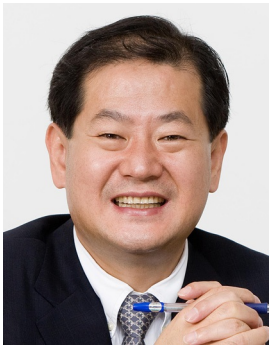

Table 1. TON and yield in photocatalytic water oxidation by persulfate using homogeneous catalysts.

Catalyst	pH	TON[a]	Yield [%][b]	Ref.
$[Fe_{11}(H_2O)_{14}(OH)_2(W_3O_{10})_2(\alpha\text{-}SbW_9O_{33})_6]^{27-}$[c]	10.0	1815	94	[41]
$[Co^{II}_3Ho(hmp)_4(OAc)_5H_2O]$[d,e]	8.0	99	97	[42]
$[Co^{II}_3Er(hmp)_4(OAc)_5H_2O]$[d,e]	8.0	93	91	[42]
$[Co^{II}_3Tm(hmp)_4(OAc)_5H_2O]$[d,e]	8.0	40-72	>90	[42]
$[Co^{II}_3Yb(hmp)_4(OAc)_5H_2O]$[d,e]	8.0	76	97	[42]
$[Co^{II}_4(hmp)_4(\mu\text{-}OAc)_2(\mu_2\text{-}OAc)_2(H_2O)_2]$[d,e]	8.0	29	96	[43]
$[(A\text{-}\alpha\text{-}SiW_9O_{34})_2Co_8(OH)_6(H_2O)_2\text{-}(CO_3)_3]^{16-}$ (Co_8POM)	9.0	1436	44	[44]
$[\{Ru_4O_4(OH)_2(H_2O)_4\}(\gamma\text{-}SiW_{10}O_{36})_2]^{10-}$	7.2	350	38	[45]
$Na_{50}[Ni_{25}(H_2O)_2(OH)_{18}(CO_3)_2(PO_4)_6(SiW_9O_{34})_6]\cdot 85H_2O$	9.0	125	18	[46]
$[\{Co_4(OH)_3(PO_4)\}_4(GeW_9O_{34})_4]^{32-}$	9.0	39	31	[47]
$[\{Co_4(OH)_3(PO_4)\}_4(AsW_9O_{34})_4]^{28-}$	9.0	33	26	[47]
$Na_{10}[Co_4(H_2O)_2(VW_9O_{34})_2]\cdot 35H_2O$	9.0	750	60	[48]
$Co_3(O_3PCH_2\text{-}NC_4H_7\text{-}CO_2)_2\cdot 4H_2O$	9.0	10	78	[49]
$[Mn^{III}_3Mn^{IV}O_3(CH_3COO)_3(A\text{-}\alpha\text{-}SiW_9O_{34})]^{6-}$	5.2	5.2	3.7	[50]
$K_{10}[Co(H_2O)_2(\gamma\text{-}SiW_{10}O_{35})_2]\cdot 23H_2O$	9.0	187	58	[51]
$Cs_9[(\gamma\text{-}PW_{10}O_{36})_2Ru^{IV}_4O_5(OH)(OH_2)_4]$	5.8	120	25	[52]
$(NH_4)_3[CoMo_6O_{24}H_6]\cdot 7H_2O$	8.0	107	26	[53]
$(NH_4)_6[Co_2Mo_{10}O_{38}H_4]\cdot 7H_2O$	8.0	154	20	[53]
$[Co^{II}(Py5OH)(Cl)](BF_4)$[f]	8.0	51	34	[54]
$[Co_2(spy)_2](ClO_4)_4$[g]	8.5	442	5.6	[55]
CoTPPS[h]	11	122	49	[56]
CoFPS[i]	9.0	570	60	[57]
$[Co(qpy)(OH_2)_2]^{2+}$[j]	8.0	160	67	[58]
[Ru(bda)(ppy)$_2$][k]	7.1	267	80	[59]
[Ru(bda)L_2][l]	7.0	518	50	[60]
$[Ru(bda)L_2\text{-}[(Ru(bpy)_3)^{2+}]_2$[m]	7.0	210	41	[61]
$[Ru(NPM)(H_2O)(pic)_2]^{2+}$[n]	7.0	103	18	[62]
$[Fe(TAML)]^{-}$[o]	8.7	220	44	[63]
$[(V^{IV}_5V^{V}_1)O_7(OCH_3)_{12}]^{-}$	7.0	67	20	[64]
$Na[\{Ru^{II}(py\text{-}SO_3)_2(H_2O)\}_2(\mu\text{-Mebbp})]$	7.0	5300	22	[65]
$[Co_2(\mu\text{-}OH)_2(TPA)_2](ClO_4)_4$[p]	9.3	742	72	[66]

[a] TON is defined as the total number of moles of O_2 per mole of the catalyst. [b] Yield is defined as twice the number of moles of O_2 per mole of $Na_2S_2O_8$. [c] LED lamp ($\lambda \geq 420$ nm), 1.0 mM $[Ru(bpy)_3](ClO_4)_2$ (1.0 mM), $Na_2S_2O_8$ (5.0 mM), total reaction volume is 16 mL and overall volume is ca. 21 mL, sodium borate buffer (80 mM, initial pH 10.0), and vigorous agitation using a magnetic stirrer. Room temperature: 25 °C. [d] hmp = 2-(hydroxymethyl)pyridine. [e] Typical conditions: a 470 nm high flux LED (26.1 mW/cm^2), $[Ru(bpy)_3]^{2+}$ (1.0 mM), $Na_2S_2O_8$ (5.0 mM), 8 mL of a borate buffered solution (pH 8.0). [f] Py5 = 2,6-bis(methoxydi(pyridin-2-yl)methyl)-pyridine. [g] spy = 2,2′:6′,2″:6″,2‴:6‴,2⁗:6⁗,2⁗′-sexipyridine. [h] CoTPPS = (5,10,15,20-tetrakis(4′-sulfonatophenyl)porphinato) cobalt(II) tetra sodium salt. [i] CoFTS = a fluorinated cobalt porphyrin. [j] qpy = 2,2′:6′,2″:6″,2‴-quaterpyridine. [k] H_2bda = 2,2′-bipyridine-6,6′-dicarboxylic acid; ppy = 4-phenylpyridine. [l] L = *N*-cyclic aromatic ligands. [m] Two Ru^{II}-polypyridine photosensitizers are covalently linked to one [Ru(bda)L_2] catalyst. [n] NPM = 4-*tert*-butyl-2,6-di-(1′,8′-naphthyrid-2′-yl)pyridine, pic = 4-picoline. [o] TAML = tetraamido macrocyclic ligand. [p] TPA = tris(2-pyridylmethyl)amine.

quantum yield [(initial O_2 formation rate)/(photon flux)] of 47% is also the highest value ever reported for the homogeneous photocatalytic water oxidation because the quantum yield of 50% corresponds to 100% quantum efficiency (two photons are required to produce four equivalents of $[Ru(bpy)_3]^{3+}$, which oxidize water to O_2 with WOC).[41] Isotope-labeling water oxidation experiments using ^{18}O-enriched water instead of $H_2{}^{16}O$ demonstrated that the evolved oxygen comes from water-derived oxygen atoms.[41] In catalytic water oxidation, homogeneous metal complexes are often claimed as precatalysts, which decompose under oxidizing conditions to insoluble metal oxides that are the real catalysts as discussed in the next section. Dynamic light scattering (DLS) measurements indicate that no nanoparticles are produced during the photocatalytic water oxidation with the POM, which remains as a soluble homogeneous catalyst.[41]

Inspired by the $\{CaMn_4O_5\}$ oxygen-evolving complex of photosystem II where Ca^{2+} plays the essential role,[70,71] the $[Co^{II}_3Ln(hmp)_4(OAc)_5H_2O]$ (Ln = Ho–Yb, hmp = 2-(hydroxymethyl)pyridine) cubane complexes were designed to address crucial design parameters, ranging from nuclearity and redox-inactive promoters by newly combining Ln^{3+} centers as redox-inactive Ca^{2+} analogues with flexible aqua-/acetate ligands into active and stable WOCs, which afforded high O_2 yields in the photocatalytic water oxidation by persulfate (Table 1).[42,43]

The catalytic mechanism was reported for the water oxidation by ceric ammonium nitrate (CAN), $(NH_4)_2[Ce^{IV}(NO_3)_6]$, using all-inorganic mononuclear ruthenium complexes bearing a Keggin-type lacunary heteropolytungstate, $[Ru^{III}(H_2O)SiW_{11}O_{39}]^{5-}$ and $[Ru^{III}(H_2O)GeW_{11}O_{39}]^{5-}$, as WOCs.[72] It has been proposed that the $Ru^{V}=O$ species was produced by the two-electron oxidation of the Ru^{III} complex with two equivalents of CAN (Scheme 3).[72] The formation of the $Ru^{V}=O$ complex was indeed detected by EPR and resonance Raman spectroscopy.[72]

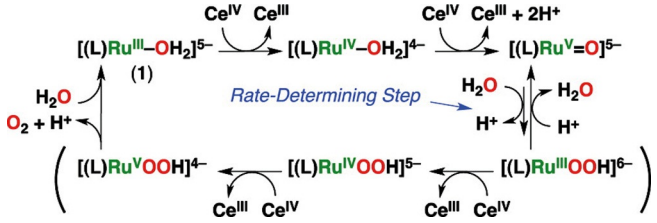

Scheme 3. Catalytic cycle for thermal water oxidation with CAN using $[(L)Ru^{III}\text{-}OH_2]$, $([Ru^{III}(H_2O)SiW_{11}O_{39}]^{5-}$, and $[Ru^{III}(H_2O)GeW_{11}O_{39}]^{5-})$, as WOCs.

A kinetic study suggested that the rate-determining step (r.d.s.) is the nucleophilic attack of H_2O to the $Ru^{V}=O$ complex to produce the $Ru^{III}OOH$ complex, which is the O–O bond formation step, where the reverse O–O bond cleavage process is in competition with the follow-up two-electron oxidation processes to generate O_2 (Scheme 3).[72]

Virtually, the same mechanism, as shown in Scheme 4, was proposed for the photocatalytic water oxidation by persulfate using a water-soluble cobalt porphyrin (CoFPS), which possesses fluorine groups at the 2- and 6-positions of the *meso*-aryl rings of the porphyrin (Scheme 4). CoFPS exhibited significantly improved stability with a high TON (570) as compared with non-fluorinated Co porphyrin (CoTPPS: TON = 122).[56] The increased stability results from resistance of CoFPS against singlet oxygen, the formation of which was monitored in situ by using 9,10-diphenylanthracene as a chemical probe.[57] DLS indicated that CoFPS remained homogeneous during the water oxidation catalysis.[57] In the case of the photocatalytic oxidation, two equivalents of $[Ru(bpy)_3]^{3+}$ produced by the oxida-

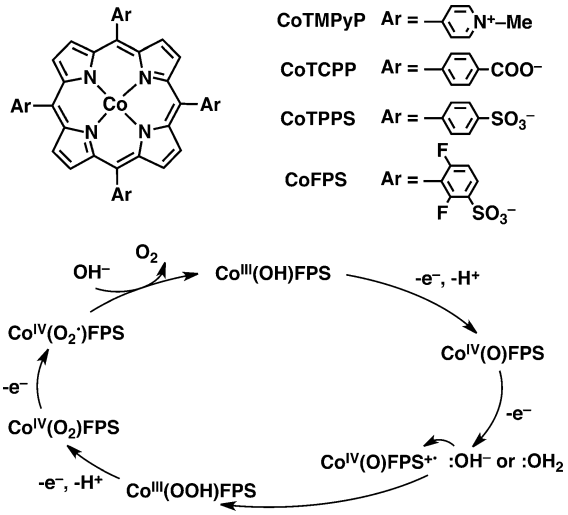

Scheme 4. Catalytic cycle for photodriven water oxidation by persulfate using CoFPS as a WOC.

tive quenching of $[Ru(bpy)_3]^{2+*}$ by persulfate (Scheme 1) can oxidize Co^{III}FPS to produce $Co^{IV}(O)FPS^{\bullet+}$, which is equivalent to $Co^{V}(O)$FPS (Scheme 4). The nucleophilic attack of water to $Co^{V}(O)$FPS affords the hydroperoxo complex ($[Co^{III}(OOH)FPS]^-$), which is further oxidized by two equivalents of $[Ru(bpy)_3]^{3+}$ to produce O_2 and regenerate Co^{III}FPS (Scheme 4). The nucleophilic attack of water to high-valent cobalt-oxo species has also been proposed for electrocatalytic water oxidation with Co hangman corroles,[73] non-heme Co complexes,[74] and cationic Co porphyrins.[75]

When a Ru^{III}-aqua complex, $Ru(\kappa_3\ ^{O,N,N}bda)(L)_2(OH_2)$ (L = 6-F-isoquinoline), was employed as a WOC for the water oxidation by CAN, a $Ru^{V}=O$ species produced by the oxidation of Ru^{III}-OH_2 by two equivalents of CAN was proposed to undergo radical coupling to produce the dinuclear peroxo complex (Ru^{IV}-O-O-Ru^{IV}), as shown in Scheme 5.[76] O_2 may be evolved directly

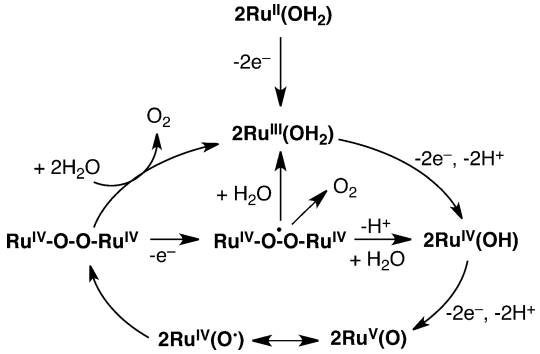

Scheme 5. Catalytic cycle for water oxidation by CAN with a Ru^{III}-aqua complex (Ru-OH_2: $[Ru(\kappa_3{}^{O,N,N}bda)(L)_2(OH_2)]$ (L = 6-F isoquinoline)).

by the reaction of Ru^{IV}-O-O-Ru^{IV} with water or Ru^{IV}-O-O-Ru^{IV} is further oxidized to a superoxo complex which reacts with H_2O to evolve O_2, accompanied by regeneration of Ru^{III}-OH_2 and Ru^{IV}-OH (Scheme 5). The radical coupling process may be the rate-determining step in the catalytic water oxidation with CAN because the rate of water oxidation was proportional to the square of the concentration of Ru^{III}-OH_2.[76] The formation of the radical superoxo intermediate $[Ru^{IV}$-O-O-$Ru^{IV}]^{\bullet 3+}$ was indicated in the electrochemical experiments and supported by DFT calculations.[76] However, the direct detection of the intermediates has yet to be made. [Ru(bda)(6-fluoroisoquinoline)$_2$] showed an extremely high catalytic activity with a TOF of 1000 s^{-1}, whereas [Ru(bda)(6-bromophthalazine)$_2$] exhibited a high TON (~100 000).[76]

A large TON (5300) was obtained in the photocatalytic water oxidation by persulfate with a ruthenium tris(bipyridyl)-type dye (RuPS) and a pyrazolate-based dinuclear ruthenium water oxidation catalyst, $\{[Ru^{II}(py\text{-}SO_3)_2(H_2O)]_2(\mu\text{-Mebbp})\}^{-}$, at pH 7.0 (Table 1).[65,77] The mechanism of O–O bond formation (nucleophilic attack of water in Schemes 3 and 4 versus radical coupling in Scheme 5) in the catalytic water oxidation can be controlled by the relative position of the Ru-O units, in addition to the electronic effects exerted by the auxiliary ligands.[13,78–80]

A radical coupling mechanism was also proposed for the O–O bond formation in the photocatalytic water oxidation by persulfate with $[Ru(bpy)_3]^{2+}$ and CoTPPS, as shown in Scheme 6.[56] The observation of a second-order dependence of the rate on the concentration of CoTPPS in the photocata-

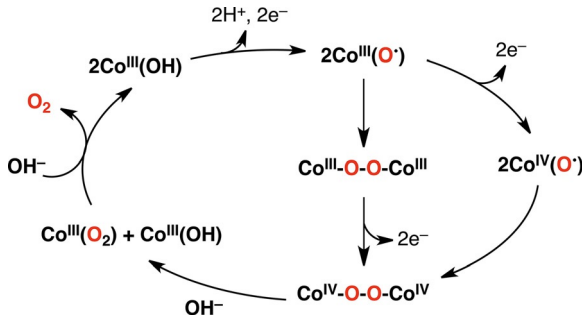

Scheme 6. Catalytic cycle for photodriven water oxidation by persulfate with $[Ru(bpy)_3]^{2+}$ as a photocatalyst and CoFPS as a WOC.

lytic water oxidation by persulfate indicates that the radical coupling of two Co-oxyl radicals is the rate-determining step in Scheme 6.[56] The change in the O–O bond formation mechanism from the nucleophilic attack of water to the $Co^{V}(O)$ species (or $Co^{IV}(O)$ porphyrin radical cation) of CoFPS in Scheme 4 to the radical coupling of the $Co^{IV}(O)$ species of CoTPPS in Scheme 6 was suggested on the basis of the observation of a less steric effect in CoTPPS relative to CoFPS owing to the shift of the sulfate groups from the 3- to the 4-positions on the aryl rings for the bimolecular radical coupling reaction.[57] The calculated Mulliken spin densities at the oxo ligand for the formally Co^{V} complexes show that CoFPS has more radical character on the oxyl oxygen (spin = 1.42) than CoTPPS does (spin = 1.09), thus suggesting that CoFPS may be more efficient at bimolecular radical coupling.[57] However, the electronic effect seems to be less important in the catalytic water oxidation with cobalt porphyrins. Any intermediates in Scheme 6 have yet to be detected or identified.

A bis-hydroxo-bridged dinuclear Co^{III}-pyridylmethylamine complex, $[\{Co(TPA)\}_2(\mu\text{-}OH)_2]^{4+}$ (**1**), acts as a homogeneous catalyst for photocatalytic water oxidation by persulfate with $[Ru(bpy)_3]^{2+}$, affording a high quantum yield (88%) and chemical yield (72%) with a high turnover number (TON = 742) for O_2 formation (Table 1) without forming catalytically active Co-oxide (CoO_x) nanoparticles.[66] The pH dependence of the catalytic activity indicates that the active species of water oxidation is a species (**2**) derived from the two-electron PCET oxidation of **1** and that the PCET formation of **2** is the rate-determining step of the water oxidation, as shown in Scheme 7.[66] The DFT calculations suggest that the most stable state of **2** is the triplet state of the bis-μ-oxyl Co^{III}-dinuclear complex, $[Co^{III}_2(\mu\text{-}O^{\cdot-})_2(TPA)_2]^{4+}$, rather than a bis-μ-oxo-Co^{IV} dinuclear complex.[66] The bis-μ-oxyl-Co^{III}_2 complex in the singlet state is thermally accessible on the basis of the result, suggesting that the singlet species is only 0.5 kcal mol^{-1} higher than the triplet state, being converted thermally to a putative $\mu{:}\eta^2,\eta^2$-peroxo-Co^{III} dinuclear complex, the energy of which is only by 0.7 kcal mol^{-1} higher than that of the singlet bis-μ-oxyl-Co^{III}_2 complex.[66] Based on isotope-labeling experiments, the O—O bond formation has been proposed to occur via intramolecular radical coupling between the two oxyl ligands locating diagonally in the singlet $Co^{III}_2(\mu\text{-}O^{\cdot-})_2$ rectangular core to afford the putative $\mu{:}\eta^2,\eta^2$-peroxo-Co^{III} intermediate, which reacts with water to produce a proposed μ-peroxo-μ-hydroxo dinuclear Co^{III} complex (**3**).[66] The complex **3** is further oxidized to evolve O_2, accompanied by regeneration of **1** (Scheme 7).[66]

3. Heterogeneous Catalysts Derived from Molecular Precatalysts

As mentioned above, determination of the true catalyst for the water oxidation to dioxygen has become an important issue because extra caution needs to be taken to clarify whether nanoparticles are produced from the homogeneous metal complexes throughout the oxidation reactions, acting as the actual catalysts or not.[81–93] Water-soluble cobalt complexes (Figure 1 a–d) have been reported to act as precatalysts rather than actual catalysts in the photocatalytic water oxidation by persulfate with $[Ru(bpy)_3]^{2+}$.[94] The TON and yield of O_2 are listed in Table 2. The yield of O_2 per persulfate with $[Co^{II}(Me_6tren)(OH_2)]^{2+}$ (50 μM) was 54%.[94] When the concentration of $[Co^{II}(Me_6tren)(OH_2)]^{2+}$ was increased to 2.5 mM, however, no O_2 was evolved after photoirradiation of the buffer solution containing $Na_2S_2O_8$ and $[Ru(bpy)_3]^{2+}$ (1st run) because the oxidation of the organic ligands proceeded prior to water oxidation to produce CO_2 rather than O_2.[94] Particles formed at the 1st run were separated from the reaction solution by centrifugation, washed successively with water and ethanol, and dried in vacuo at room temperature.[94] When the particles (~0.12 mg) were employed as a catalyst at the 2nd run, efficient O_2 evolution (~60% yield) was observed.[94] Robustness of the nanoparticles was confirmed by collecting them after each catalytic cycle and by re-using them in a subsequent catalytic cycle. Actually, a significant amount of O_2 evolution could be observed even in the 3rd cycle.[94] Thus, the actual catalyst for the photocatalytic water oxidation was the particles derived from $[Co^{II}(Me_6tren)(OH_2)]^{2+}$.[94] The nanoparticle formation was confirmed by DLS measurements, which indicate that the aver-

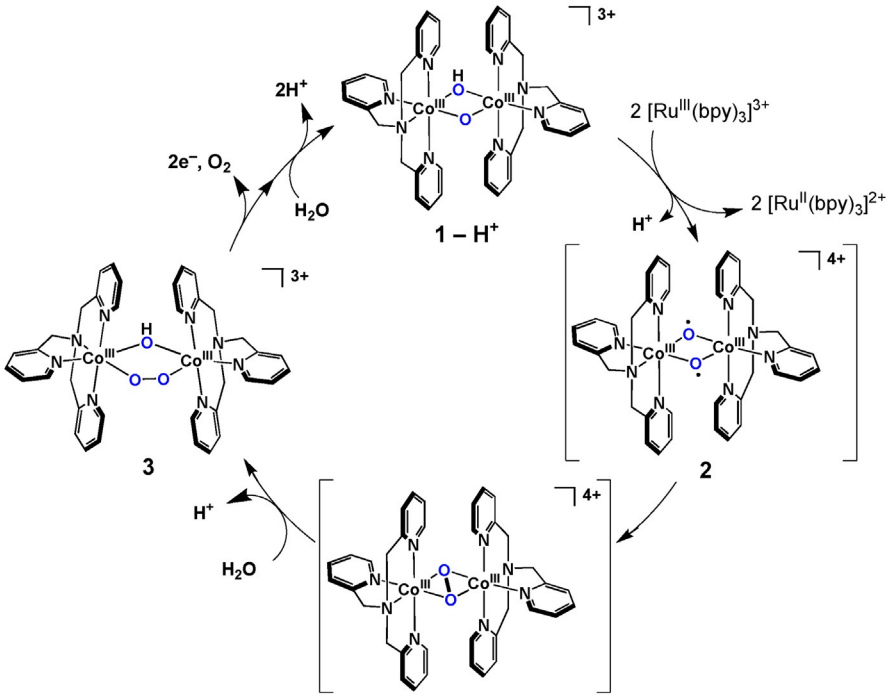

Scheme 7. Catalytic cycle for photodriven water oxidation at pH 9.3 by persulfate with $[Ru(bpy)_3]^{2+}$ as a photocatalyst and a bis-μ-hydroxo-Co^{III}-TPA dinuclear complex, $[\{Co(TPA)\}_2(\mu\text{-}OH)_2]^{4+}$ (**1**), as a WOC. At pH 9.3, the complex **1** is deprotonated to be the corresponding μ-oxo-μ-hydroxo form (**1**—H^+).

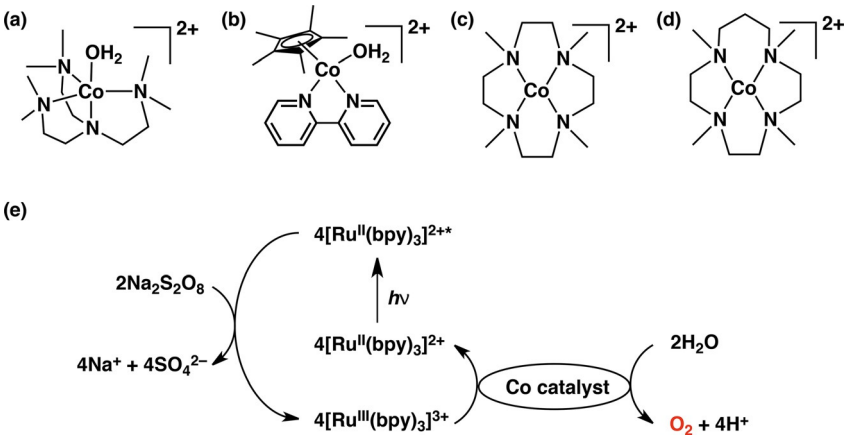

Figure 1. Chemical structures of mononuclear water-soluble cobalt complexes used as precatalysts (a) $[Co^{II}(Me_6tren)(OH_2)]^{2+}$, (b) $[Co^{III}(Cp^*)(bpy)(OH_2)]^{2+}$, (c) $[Co^{II}(12\text{-TMC})]^{2+}$, and (d) $[Co^{II}(13\text{-TMC})]^{2+}$. (e) Scheme showing the overall catalytic cycle for photocatalytic water oxidation by $Na_2S_2O_8$ with $[Ru(bpy)_3]^{2+}$ and a cobalt complex precatalyst.

Table 2. TON and yield in photocatalytic water oxidation by persulfate using homogeneous catalyst precursors.

Catalyst	pH	TON[a]	Yield [%][b]	Ref.
$[Co^{II}(Me_6tren)(OH_2)]^{2+}$[c,d]	8.0	54	54	[94]
$[Co^{III}(Cp^*)(bpy)(OH_2)]^{2+}$[c,e]	8.0	29	29	[94]
$[Co^{II}(12\text{-TMC})]^{2+}$[c,f]	8.0	16	16	[94]
$[Co^{II}(13\text{-TMC})]^{2+}$[c,g]	8.0	41	41	[94]
$Co^{II}(NO_3)_2$[c]	8.0	52	52	[94]
Co^{II}(Salen)[h]	9.0	854	55	[95]
Fe(mcp)Cl_2[i]	8.5	194	24	[97]
$[Fe(bpy)_2Cl_2]Cl$	8.5	157	21	[97]
$[Fe(tpy)_2]Cl_2$[j]	8.5	376	42	[97]
$[Fe(cyclen)Cl_2]Cl$[k]	8.5	412	46	[97]
Fe(tmc)Br_2[l]	8.5	364	41	[97]
$Fe(ClO_4)_3$	8.5	436	48	[97]
Fe(BQEN)$(OTf)_2$[m]	9.0	259	52	[98]
$[NiL_1](ClO_4)_2$[n]	8.0	2	3	[100]
$[NiL_2](ClO_4)_2$[o]	8.0	53	30	[100]
$[NiL_3](ClO_4)_2$[p]	8.0	54	31	[100]
$[NiL_4](ClO_4)_2$[q]	8.0	31	19	[100]
$[NiL_5](ClO_4)_2$[r]	8.0	41	25	[100]
$[NiL_6](ClO_4)_2$[s]	8.0	50	29	[100]
$Ni(NO_3)_2$	8.0	65	37	[100]

[a] TON is defined as the total number of moles of O_2 per mole of the catalyst. [b] Yield is defined as twice the number of moles of O_2 per mole of $Na_2S_2O_8$. [c] Typical conditions: Photoirradiation (Xe lamp, $\lambda > 420$ nm) of a buffer solution (2.0 mL, 50 mM phosphate, pH 8.0) containing $[Ru(bpy)_3]^{2+}$ (0.50 mM), $Na_2S_2O_8$ (10 mM) and a mononuclear cobalt complex (50 μM). [d] Me_6tren = tris[2-(dimethylamino)ethyl]amine. [e] Cp* = pentamethylcyclopntadienyl. [f] 12-TMC = 1,4,7,10-tetramethyl-1,4,7,10-tetraazacyclododecane. [g] 13-TMC = 1,4,7,10-tetramethyl-1,4,7,10-tetraazacyclotridecane. [h] Salen = *N*,*N*′-bis(salicylidene)ethylenediamine. [i] mcp = *N*,*N*′-dimethyl-*N*,*N*′-bis(2-pyridylmethyl)cyclohexane-1,2-diamine. [j] tpy = 2,2′:6′,2″-terpyridine. [k] cyclen = 1,4,7,10-tetraazacyclodecane. [l] tmc = 1,4,8,11-tetramethyl-1,4,8,11-tetraazacyclotetradecane. [m] BQEN = *N*,*N*′-dimethyl-*N*,*N*′-bis(8-quinolyl)ethane-1,2-diamine. [n] L_1 = *N*,*N*,*N*′*N*′-tetrakis(2-pyridylmethyl)ethylenediamine. [o] L_2 = *N*,*N*,*N*′-tris-[2-(2′-pyridyl)ethyl]-*N*′-methylethane-1,2-diamine. [p] L_3 = *N*,*N*′-bis-[2-(2′-pyridyl)ethyl]-*N*,*N*′-dimethylethane-1,2-diamine. [q] L_4 = *N*,*N*′-dimethyl-*N*,*N*′-bis(pyridyl-2yl-methyl)ethylene-diamine. [r] L_5 = *meso*-2,3,7,11,12-pentamethyl-3,7,11,17-tetra-azabicyclo[11.3.1]heptadeca-1(17),13,15-triene. [s] L_6 = 1,4,8,11-tetramethyl-1,4,8,11-tetraazacyclotetradecane.

age size of nanoparticles is 15–60 nm.[94] Transmission electron microscopy (TEM) images of the particles derived from $[Co^{II}(Me_6tren)(OH_2)]^{2+}$ are displayed in Figure 2a and 2b.[94] The size of particles ranged from 10 to 50 nm, which agrees with the range of particles size determined by DLS (15–60 nm).[94] Similar nanoparticles were formed from $[Co^{III}(Cp^*)(bpy)(OH_2)]^{2+}$ (Figure 2c and 2d) and $Co(NO_3)_2$ (Figure 2e and 2f).[94] The high magnification image in Figure 2b indicates that smaller particles in the size of few nanometers were also formed, indi-

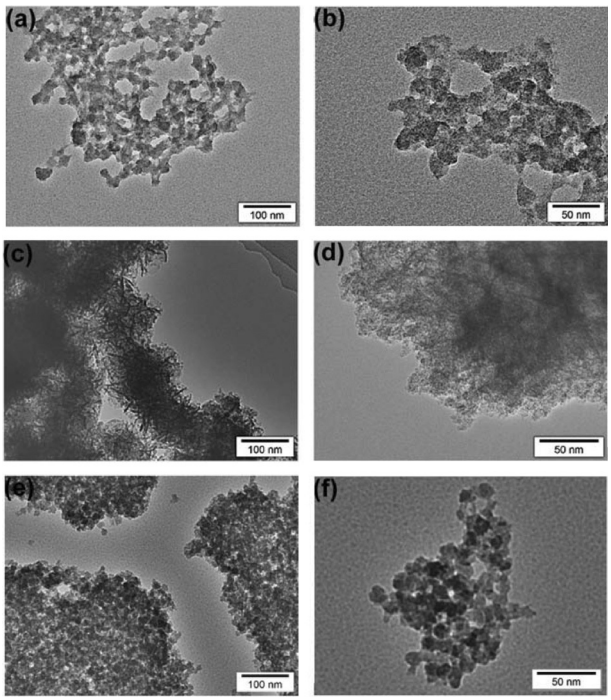

Figure 2. TEM images of nanoparticles formed during the photocatalytic water oxidation with (a and b) $[Co^{II}(Me_6tren)(OH_2)]_{2+}$, (c and d) $[Co^{III}(Cp^*)(bpy)\text{-}(OH_2)]^{2+}$, and (e and f) $Co(NO_3)_2$ in a buffer solution (pH 9) containing $[Ru(bpy)_3]^{2+}$ (0.50 mM) and $Na_2S_2O_8$ (10 mM).

cating that the particles observed in Figure 2a are secondary particles.[94]

X-ray photoelectron spectroscopy (XPS) spectra of the nanoparticles derived from $[Co^{II}(Me_6tren)(OH_2)]^{2+}$ exhibited Co $2p_{1/2}$ and Co $2p_{3/2}$ peaks at 780.0 eV and 795.3 eV, respectively, with weak satellite peaks.[94] Co_3O_4 also showed two intense peaks at 779.8 eV for Co $2p_{1/2}$ and at 795.1 eV for Co $2p_{3/2}$ with weak satellite peaks.[94] Slightly intense satellite peaks observed with the nanoparticles were ascribed to the higher ratio of Co^{II} species before the photocatalytic water oxidation.[94] The O 1s peak of the nanoparticles appeared at 531.5 eV, which is in a higher binding energy region compared with the O 1s peak of Co_3O_4 (530.3 eV) by 1.2 eV.[94] An increase in the binding energy of the O 1s peak of the nanoparticles suggests the existence of metal hydroxide species.[94] Thus, the surface of the nanoparticles derived from $[Co^{II}(Me_6tren)(OH_2)]^{2+}$ under the photocatalytic water oxidation is mainly composed of $Co(OH)_x$, which acts as the actual reactive catalyst for the photocatalytic water oxidation.[94] The organic ligands were oxidized to CO_2 during the photocatalytic water oxidation, but the carbonaceous residues may act as a modifier or capping agent of the species compared with the authentic Co_3O_4 sample because $[Co^{II}(Me_6tren)(OH_2)]^{2+}$ exclusively contained Co^{II} nanoparticles to avoid the further aggregation to maintain the catalytic reactivity.[94]

A Co^{II}(salen) complex (salen = *N,N'*-bis(salicylidene)-ethylenediamine) also acts as a highly efficient water oxidation precatalyst in the photocatalytic oxidation of water by persulfate with $[Ru(bpy)_3]^{2+}$ as a photocatalyst, affording a TON of 854 at pH 9.0 (Table 2).[95] Based on the electrospray ionization mass spectrum (ESI-MS), ^{1}H NMR and XPS analyses, the precipitates derived from Co^{II}(salen) during the photocatalytic water oxidation are composed of a mixture of Co^{III} containing oxide and/or Co^{III} hydroxide.[95] Cobalt-salen complexes were also reported to serve as precursors to deposit nanostructured amorphous catalyst films for catalytic water oxidation with high activity.[96]

Various iron complexes and $Fe(ClO_4)_3$ also act as precatalysts for the photocatalytic water oxidation by persulfate with $[Ru(bpy)_3]^{2+}$ at pH 8.5 to produce nanoparticles (Table 2), which were isolated and found to be Fe_2O_3 using various techniques, including energy-dispersive X-ray spectroscopy and XPS.[97] α-Fe_2O_3 nanoparticles prepared with a diameter of 15–70 nm exhibited a similar catalytic reactivity with a TON of 58 compared to $Fe(ClO_4)_3$ used as a precatalyst, which gave a TON of 57.[97]

In the case of $Fe(BQEN)(OTf)_2$ used as a precatalyst, nanoparticles isolated after the light-driven water oxidation by persulfate at the initial pH 9.0 were found to be iron hydroxides by XPS measurements.[98] Under acidic conditions, $Fe^{II}(BQEN)^{2+}$ is oxidized by two equivalents of CAN to produce an iron(IV)-oxo species, $[Fe^{IV}(O)(BQEN)]^{2+}$, which is further oxidized to produce O_2.[98] Thus, $Fe^{II}(BQEN)^{2+}$ acts as a homogeneous catalyst for water oxidation by CAN without formation of nanoparticles, although the dissociation of the BQEN ligand competes with the formation of $[Fe^{IV}(O)(BQEN)]^{2+}$ under acidic conditions.[98] Simple cobalt salts are reported to act as homogeneous catalysts for the photocatalytic water oxidation by persulfate under acidic conditions (pH 3.0), although the catalytic reactivity is much reduced as compared with that under basic conditions, where the catalytically more active nanoparticles are produced.[99]

A number of Ni complexes and salts (see Table 2) were also converted to nanoparticles during the photocatalytic water oxidation by persulfate pH 7–9 in borate buffer, which were found to be partially reduced β-NiOOH by scanning electron microscopy (SEM), energy-dispersive X-ray spectroscopy, XPS, X-ray diffraction (XRD), and IR spectroscopies.[100] $[Ni(en)_3]Cl_2$ (en = 1,2-diaminoethane) was also reported to serve as a precursor to deposit nanostructured amorphous nickel oxide (NiO_x), which acts as water oxidation catalysts with high catalytic activity in a 0.10 M borate buffer solution (pH 9.2).[101]

In contrast to iron complexes which act as homogeneous catalysts for water oxidation by CAN under acidic conditions (see above), iridium complexes $[Ir^{III}(Cp^*)(4,4'\text{-}R_2\text{-}2,2'\text{-bipyridine})(H_2O)]^{2+}$ (R = OH, OMe, Me or COOH) are converted to nanoparticles during the water oxidation by CAN.[80] The nanoparticles were composed of iridium hydroxide with a small amount of carbonaceous residue based on TG/DTA and XPS measurements of nanoparticles produced after the water oxidation.[80] The iridium hydroxide nanoparticles act as an excellent catalyst for the water oxidation by CAN with a high TOF (0.75 s^{-1}) and a high TON (> 1500).[80]

A water-soluble Ir complex, $[Ir(Cp^*)(H_2O)_3]^{2+}$, was used as a precatalyst for iridium hydroxide nanoparticles, which acts as an efficient water oxidation catalyst in the photocatalytic water oxidation by O_2 to produce hydrogen peroxide with $[Ru^{II}(Me_2phen)_3]^{2+}$ (Me_2phen = 4,7-dimethyl-1,10-phenanthroline) in the presence of Sc^{3+} in water under visible-light irradiation.[102] The photocatalytic cycle for H_2O_2 production from H_2O and O_2 is shown in Scheme 8, where the photoreduction of O_2

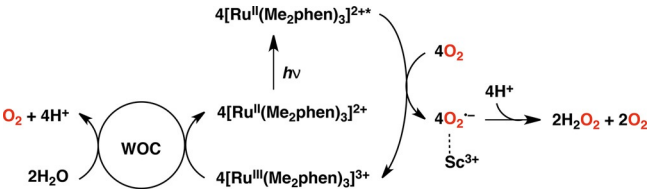

Scheme 8. Catalytic cycle for photocatalytic water oxidation by persulfate with $[Ru^{II}(Me_2phen)_3]^{2+}$ and WOC in the presence of Sc^{3+} in water.

to H_2O_2 by $[Ru^{II}(Me_2phen)_3]^{2+}$ in the presence of Sc^{3+} is combined with the catalytic water oxidation to O_2 by $[Ru^{III}(Me_2phen)_3]^{3+}$.[103] Photoinduced electron transfer from the excited state of $[Ru^{II}(Me_2phen)_3]^{2+}$ to O_2 results in the formation of $[Ru^{III}(Me_2phen)_3]^{3+}$ and $O_2^{\bullet-}$ that binds to Sc^{3+} and the disproportionation of $O_2^{\bullet-}$-Sc^{3+} in water yields H_2O_2.[104] Four equivalents of $[Ru^{III}(Me_2phen)_3]^{3+}$ can oxidize H_2O to O_2 in the presence of a WOC.[102, 103]

The time course of the photocatalytic production of H_2O_2 with $[Ru^{II}(Me_2phen)_3]^{2+}$ and $[Ir(Cp^*)(H_2O)_3]^{2+}$ in the presence of $Sc(NO_3)_3$ (100 mM) in water at various temperatures is shown

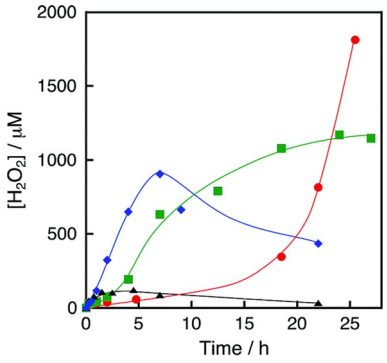

Figure 3. Time courses of H_2O_2 production under visible-light ($\lambda > 420$ nm) irradiation of $[Ru^{II}(Me_2phen)_3]^{2+}$ (20 μM) in the presence of $[Ir(Cp^*)(H_2O)_3]^{2+}$ (100 μM) and Sc^{3+} (100 mM) in an O_2-saturated aqueous solution (3.0 mL) at 333 K (black triangles), 313 K (blue diamonds), 293 K (green squares) and 278 K (red circles).

in Figure 3, where an induction period is observed in particular at 278 K.[102] The rate of formation of H_2O_2 increased rapidly after the induction period.[102] Such a sigmoidal behavior in the initial stage of H_2O_2 production with $[Ir(Cp^*)(H_2O)_3]^{2+}$ (red in Figure 3) indicates that $[Ir(Cp^*)(H_2O)_3]^{2+}$ acts as a precatalyst to produce catalytically more active nanoparticles during the photocatalytic production of H_2O_2.[102] The initial rate of H_2O_2 production increases with increasing temperature, but the maximum H_2O_2 concentration decreased because of the enhanced decomposition of H_2O_2 (Figure 3).[102] The formation of nanoparticles was confirmed by DLS measurements. The size of nanoparticles formed after 12 h photoirradiation at 278 K was 21 nm, whereas the size increased to 240 nm after 36 h photoirradiation.[102] Large-sized particles (450 nm) were obtained after 12 h photoirradiation at 333 K.[102] Thus, the size of the particles depends on the photoirradiation time and temperature. XPS measurements of the nanoparticles centrifugally recovered from the reaction solution after the H_2O_2 production reaction indicated that the formed nanoparticles were composed of $Ir(OH)_3$ as the case of water oxidation by CAN (see above).[80,102]

4. Heterogeneous Catalysts

Metal oxides, in the form of dispersed powders, have been extensively examined as heterogeneous WOCs in the photocatalytic water oxidation by persulfate with $[Ru(bpy)_3]^{2+}$ (Scheme 2).[104–122] The yields of O_2 and the activity in the catalytic water oxidation by persulfate with heterogeneous catalysts are listed in Table 3.[106–122] The most efficient metal oxide catalyst is IrO_2, which gave >99% yield of O_2 per persulfate and a rate of O_2 formation of 190 $\mu M\,s^{-1}\,g^{-1}$.[106,107] IrO_2 nanocrystals were reported to photocatalyze oxygen formation from aqueous solutions of sacrificial electron acceptors, without the use of an external light absorber such as $[Ru(bpy)_3]^{2+}$.[108] Photochemical charge carriers are formed when electrons are excited from the Ir-d(t_{2g}) to the Ir-d(e_g) band (1.5–2.75 eV) or from the O-p to the Ir-d(e_g) band (> 3.0 eV).[108] The O_2 yield in the photocatalytic water oxidation by persulfate with IrO_2 nanoparticles was 73%, which is smaller than the case with $[Ru(bpy)_3]^{2+}$ (>99%) in Table 3.[108] The rate of O_2 formation with IrO_2 alone (18 $\mu M\,s^{-1}\,g^{-1}$) is slower than that with $(Ru(bpy)_3]^{2+}$ (190 $\mu M\,s^{-1}\,g^{-1}$) in Table 3.[108]

RuO_2 supported on mesoporous silica SBA-15 (RuO_2 NP) acted as an efficient WOC in the photocatalytic water oxidation by persulfate with $[Ru(bpy)_3]^{2+}$ to afford 95% yield of O_2,[110] which is much higher than that achieved with RuO_2 (27%)[109] and RuO_2/Y-zeolite-based catalysts (31%).[111] The quantum efficiency (twice of the quantum yield) was determined to be 11.3%.[110] RuO_2 NPs have been recycled up to five times with minimal loss of activity.[110]

Table 3. TON and yield in photocatalytic water oxidation by persulfate using heterogeneous catalysts.

Catalyst	pH	Rate[a]	Yield [%][b]	Ref.
IrO_2	5.4[c]	190	>99	[106]
IrO_2[d]	10	18	73	[108]
RuO_2	5.0	–	27	[109]
RuO_2 NP[e]	5.4	–	95	[110]
RuO_x/Y-zeolite[f]		–	31	[111]
$NiFe_2O_4$[g]	8.0	2.7	74	[112]
Co_3O_4[g]	8.0	2.4	64	[112]
Co_3O_4-150[h]	7.0	-	27	[113]
Co_3O_4-750[h]	7.0	-	16	[113]
NiO[g]	8.0	1.5	52	[112]
α-NiO nanorods[i]	8.5	1.8	44	[114]
Fe_3O_4[g]	9.0	0.95	55	[112]
Fe_2O_3[g]	8.5	0.65	24	[112]
Fe_2O_3 (nanocubes)	8.0	–	13.4	[115]
Fe_2O_3 (nanoplates)	8.0	–	4.5	[115]
Fe_2O_3 (nanoflakes)	8.0	–	3.0	[115]
Fe_2O_3 (nanoarticle)	8.0	–	17.7	[115]
$CuFe_2O_4$	8.5	11	73	[116]
$LaCoO_3$	7.0	5.5	74	[117]
$CoWO_4$[j]	7.0	1.3	19	[117]
$La_{0.7}Sr_{0.3}CoO_3$[j]	7.0	3.6	59	[117]
$NdCoO_3$[j]	7.0	4.6	59	[117]
$YCoO_3$[j]	7.0	1.8	24	[117]
CoNCN[k]	9.0	–	76	[118]
$NiMnO_3$	7.0	9.6	52	[119]
α-MnO_2	7.0	5.0	24	[119]
Mn_2O_3	7.0	2.5	18	[119]
Mn_2O_3 (bixbyite)	7.0	2.4	–	[120]
Mn_3O_4	7.0	1.0	4	[119]
Mn_3O_4 ((hausmannite)	7.0	1.0	–	[120]
γ-MnO_2	7.0	0.94	–	[120]
$NiO/CoO/Fe_2O_3$	8.5	–	64	[121]
$NiO + CoO + Fe_2O_3$	8.5	–	47	[121]
$[Co^{II}(H_2O)_{1.79}]_{1.42}[(Co^{III}_{0.85}Pt^{IV}_{0.15})(CN)_6]$	8.0	62	100	[125]

[a] O_2 evolution rate: $\mu M\,s^{-1}\,g^{-1}$ (catalyst weight: g). [b] Yield is defined as twice the number of moles of O_2 per mole of $Na_2S_2O_8$. [c] 5.0×10^{-2} M (1.0:1.3) Na_2SiF_6-$NaHCO_3$ buffer. [d] Photoirradiation (300 W Xe lamp, $\lambda >$ 400 nm) of a buffer solution (100 mL, pH 10) containing $Na_2S_2O_8$ (42.9 μmol) and IrO_2 (3.7 mg). [e] RuO_2 supported on mesoporous silica SBA-15. [f] Obtained starting from zeolite Y and $Ru_3(CO)_{12}$. [g] Photoirradiation ($\lambda > 420$ nm) of an aqueous buffer solution (pH 8.0, 2.0 mL) containing the catalyst (0.50 $g\,L^{-1}$), $Na_2S_2O_8$ (5.0 mM), and $[Ru(bpy)_3]^{2+}$ (0.25 mM). [h] The number denotes the calcination temperature. [i] α-NiO nanowires and α-NiO nanoplates exhibited similar catalytic reactivity. [j] Photoirradiation (Xe lamp, $\lambda > 420$ nm) of a phosphate buffer solution (50 mM, 2.0 mL, pH 7.0) containing the catalyst (0.25 $g\,L^{-1}$), $Na_2S_2O_8$ (5.0 mM), and $[Ru(bpy)_3]^{2+}$ (0.25 mM). [k] Cobalt carbodiimide.

Among earth-abundant metal oxide WOCs, $NiFe_2O_4$ exhibited the highest catalytic activity to afford 74% yield of O_2, which is higher than those of cobalt oxides, iron oxides, and nickel oxides (Table 3).[112–115] $NiFe_2O_4$ can be easily collected from the solution after the reaction because of its ferromagnetic properties.[112] The high O_2 yield with $NiFe_2O_4$ was maintained even after the 10th run in 5 h (Figure 4). No significant change in either the powder X-ray diffraction (PXRD) pattern or the morphology of the $NiFe_2O_4$ catalyst was observed after the water oxidation reaction.[112] Cyclic voltammetry studies of electrocatalytic water oxidation with $NiFe_2O_4$ suggested that a high-valent nickel species may be the active species for the photocatalytic water oxidation.[112]

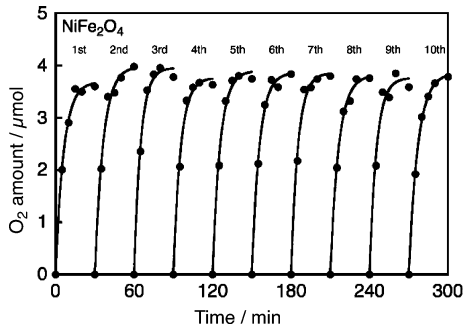

Figure 4. Time courses of O_2 evolution under photoirradiation (Xe lamp, $\lambda > 420$ nm) of a phosphate buffer solution (pH 8.0, 2.0 mL) containing $Na_2S_2O_8$ (5.0 mM) and $[Ru(bpy)_3]SO_4$ (0.25 mM) with $NiFe_2O_4$ (0.50 g L^{-1}) at room temperature in 10 repetitive examinations.

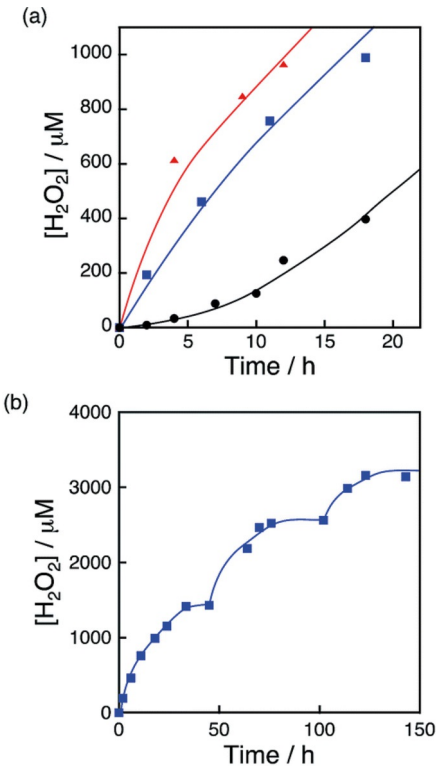

Figure 5. (a) Time courses of H_2O_2 production under visible-light irradiation ($\lambda > 420$ nm) of $[Ru^{II}(Me_2phen)_3]^{2+}$ (200 μM) in the presence of Sc^{3+} (100 mM) and $NiFe_2O_4$ (0.17 g L^{-1}) with diameters of 1300 nm (black circles), 120 nm (blue squares), and 91 nm (red triangles) in O_2-saturated H_2O (3.0 mL, $[O_2] = 1.2$ mM). (b) Time course of H_2O_2 production in the presence of $NiFe_2O_4$ (0.17 g L^{-1}) and Sc^{3+} (100 mM) under visible-light irradiation ($\lambda > 420$ nm) of $[Ru^{II}(Me_2phen)_3]^{2+}$ (200 μM) in O_2-saturated H_2O (3.0 mL, $[O_2] = 1.2$ mM). $[Ru^{II}(Me_2phen)_3]^{2+}$ was added twice to the reaction suspension at 50 h and 100 h during photoirradiation. The amount of $[Ru^{II}(Me_2phen)_3]^{2+}$ added each time at 50 h and 100 h to the reaction suspension was calculated in terms of the concentration increase of 200 μM.

The initial rate of H_2O_2 production with $NiFe_2O_4$ nanoparticles with diameters of 120 nm and 91 nm was accelerated 22 times and 33 times, respectively, as compared to the as-prepared $NiFe_2O_4$ with diameter of 1300 nm (Figure 5).[102] This increase in reactivity results from an increase in the surface area with decreasing the diameter size. The linear relationship between the initial rates of H_2O_2 production and the surface areas of $NiFe_2O_4$ nanoparticles indicates that the reactivity of each active site for water oxidation in the surface of $NiFe_2O_4$ remains unchanged irrespective of the particle size.[102]

In order to reuse the nanoparticles after H_2O_2 production ceased, an aliquot of an aqueous solution containing a high concentration of $[Ru^{II}(Me_2phen)_3]^{2+}$ was added to the reaction suspension repeatedly, in which the amount of $[Ru^{II}(Me_2phen)_3]^{2+}$ added to the starting suspension at each run was calculated in terms of the concentration increase of 200 μM. The concentration of H_2O_2 in the resulting suspension increased to be as high as 3.3 mM, ensuring the high stability of the nanoparticles as WOCs (Figure 5b).[102]

$CuFe_2O_4$ nanocrystals with cubic jacobsite structure also exhibited high catalytic activity in the photocatalytic water oxidation by persulfate with $[Ru(bpy)_3]^{2+}$ to afford 73% O_2 yield (Table 3). As in the case of $NiFe_2O_4$ (see above), $CuFe_2O_4$ can be easily separated from the reaction solution by magnetic separation while maintaining excellent water oxidation activity in the fourth and fifth runs.[116] The catalytic activity of cobalt-containing metal oxides, such as perovskites ($LaCoO_3$, $NdCoO_3$, $YCoO_3$, $La_{0.7}Sr_{0.3}CoO_3$), spinel (Co_3O_4) and wolframite ($CoWO_4$), was compared in the photocatalytic water oxidation by persulfate with $[Ru(bpy)_3]^{2+}$ (Table 3).[117] The catalysts with the perovskite structure exhibited higher catalytic activity as compared with those of the spinel and wolframite structures.[117] Among them, $LaCoO_3$ acts as the best catalyst to afford the highest O_2 yield (74%).[117] Ni^{2+} ion-doped manganese oxide ($NiMnO_3$) also exhibited high catalytic activity in the photocatalytic water oxidation by persulfate with $[Ru(bpy)_3]^{2+}$ to yield 52% O_2 yield as compared with manganese oxides.[119,120]

Recently, coordination polymers emerged as potential candidates, possessing both designable structures at the atomic level and robustness under harsh reaction conditions.[122,123] Heteropolynuclear cyanide complexes are the simplest class of coordination polymers. In general, heteropolynuclear cyanide complexes have a cubic structure as far as the contained metal ions allow octahedral coordination.[124] Heteropolynuclear cyanide complexes can be easily modified as heterogeneous catalysts suitable for water oxidation. A series of heteropolynuclear cyanide complexes containing Pt^{IV} ions, $[Co^{II}(H_2O)_m]_n[(Co^{III}_{1-x}Pt^{IV}_x)(CN)_6]$, were prepared by mixing an

aqueous solution containing both $K_3[Co^{III}(CN)_6]$ and $K_2[Pt^{IV}(CN)_6]$ with various Co^{III}/Pt^{IV} ratios ranging from 1:0 to 0:1, and an aqueous solution containing an excess amount of $Co(NO_3)_2$.[125]

Powder X-ray diffraction patterns for the heteropolynuclear cyanide complexes with the Pt^{IV} ion content ranging from 0 to 1 (Figure 6a) were assigned as a cubic structure (Figure 6b), which is often called as Prussian blue. The gradual decrease of the diffraction peaks in the 2θ angle in accordance with the increase in the Pt^{IV} ion content reflects the expansion of a unit cell resulting from the larger ionic radii of a Pt^{IV} ion (0.77 Å) relative to that of a Co^{III} ion (0.69 Å).[126]

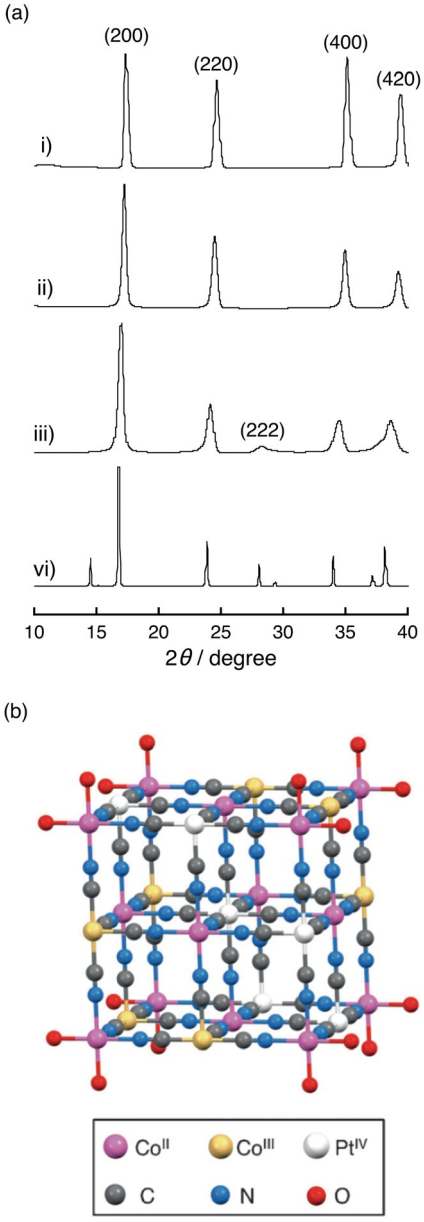

Figure 6. (a) Powder X-ray diffraction patterns of a series of heteropolynuclear cyanide complexes, $[Co^{II}(H_2O)_m]_n[Co^{III}_{1-x}Pt^{IV}_x(CN)_6]$; i) $x=0$, ii) $x=0.15$, iii) $x=0.43$, and iv) $x=1$. (b) A schematic drawing of $[Co^{II}(H_2O)_m]_n[Co^{III}_{1-x}Pt^{IV}_x(CN)_6]$. Hydrogen atoms of water molecules are omitted.

The stoichiometric amount of O_2 (100%) was obtained in the photocatalytic oxidation by persulfate with $[Ru(bpy)_3]^{2+}$ using $[Co^{II}(H_2O)_{1.79}]_{1.42}[(Co^{III}_{0.85}Pt^{IV}_{0.15})(CN)_6]$ ($x=0.15$) as a WOC at pH 8.0.[125] The initial O_2 evolution rate increases with an increase in the Pt^{IV} ion content in $[Co^{II}(H_2O)_m]_n[(Co^{III}_{1-x}Pt^{IV}_x)(CN)_6]$ to reach the maximum using $[Co^{II}(H_2O)_{1.79}]_{1.42}[(Co^{III}_{0.85}Pt^{IV}_{0.15})(CN)_6]$ as a WOC at the rate exceeded 10 nmol s^{-1}, which is comparable to that reported for most active IrO_2 nanoparticles.[49,125] Thus, the addition of $Pt^{IV}(CN)_6^{2-}$ units to cobalt cyanide complexes enhanced the catalytic activity for water oxidation by increasing the oxidation potential of *N*-bound Co^{II} ions acting as active sites through electronic and structural modifications.[125]

5. Conclusion

Homogeneous WOCs in the photocatalytic water oxidation by persulfate ($Na_2S_2O_8$) with $[Ru(bpy)_3]^{2+}$ provided valuable insights into the catalytic mechanisms, including intermediates such as metal-oxo and dinuclear metal-peroxo complexes. Whether O–O bond formation occurs by the nucleophilic attack of water to metal-oxo species or radical coupling of metal-oxo species depends on the types of metals and ligands. Whether metal complexes remain homogeneous or whether they are converted to heterogeneous nanoparticles is determined by the type of metals, ligands and water oxidation conditions, in particular by pH. This Focus Review is hoped to facilitate the understanding of catalysis of homogeneous and heterogeneous WOCs and their combinations in water oxidation reactions.

Acknowledgements

The authors gratefully acknowledge the contributions of their collaborators and coworkers mentioned in the cited references, and support by ALCA and SENTAN projects (to S.F.) from Japan Science and Technology Agency (JST), Japan, JSPS KAKENHI (Grant Nos. 24350069 and 15K14223 to Y.Y., 24655044 to T. K.), and the NRF of Korea through CRI (NRF-2012R1A3A2048842 to W.N.) and GRL (NRF-2010-00353 to W.N.).

Keywords: heterogeneous catalysis · homogeneous catalysis · nanoparticles · photocatalysis · water oxidation

[1] E. W. McFarland, *Energy Environ. Sci.* **2014**, *7*, 846–854.
[2] T. A. Faunce, W. Lubitz, A. W. (Bill) Rutherford, D. MacFarlane, G. F. Moore, P. Yang, D. G. Nocera, T. A. Moore, D. H. Gregory, S. Fukuzumi, K. B. Yoon, F. A. Armstrong, M. R. Wasielewski, S. Styring, *Energy Environ. Sci.* **2013**, *6*, 695–698.
[3] N. S. Lewis, D. G. Nocera, *Proc. Natl. Acad. Sci. USA* **2006**, *103*, 15729–15735.
[4] D. Kim, K. K. Sakimoto, D. Hong, P. Yang, *Angew. Chem. Int. Ed.* **2015**, *54*, 3259–3266; *Angew. Chem.* **2015**, *127*, 3309–3316.
[5] S. Fukuzumi, K. Ohkubo, T. Suenobu, *Acc. Chem. Res.* **2014**, *47*, 1455–1464.
[6] S. Fukuzumi, K. Ohkubo, *J. Mater. Chem.* **2012**, *22*, 4575–4587.
[7] D. Gust, T. A. Moore, A. L. Moore, *Acc. Chem. Res.* **2009**, *42*, 1890–1898.
[8] S. Fukuzumi, *Phys. Chem. Chem. Phys.* **2008**, *10*, 2283–2297.
[9] M. R. Wasielewski, *Acc. Chem. Res.* **2009**, *42*, 1910–1921.

[10] S. Fukuzumi, T. Kojima, *J. Mater. Chem.* **2008**, *18*, 1427 – 1439.
[11] G. Knör, *Coord. Chem. Rev.* **2015**, *304 – 305*, 102 – 108.
[12] S. Fukuzumi, *Curr. Opin. Chem. Biol.* **2015**, *25*, 18 – 26.
[13] S. Berardi, S. Drouet, L. Francàs, C. Gimbert-Suriñach, M. Guttentag, C. Richmond, T. Stoll, A. Llobet, *Chem. Soc. Rev.* **2014**, *43*, 7501 – 7519.
[14] S. Fukuzumi, *Biochim. Biophys. Acta* **2015**, in press, DOI: 10.1016/j.bbabio.2015.08.012.
[15] J. R. McKone, N. S. Lewis, H. B. Gray, *Chem. Mater.* **2014**, *26*, 407 – 414.
[16] S. Fukuzumi, Y. Yamada, *Aust. J. Chem.* **2014**, *67*, 354 – 364.
[17] J. Ran, J. Zhang, J. Yu, M. Jaroniec, S. Z. Qiao, *Chem. Soc. Rev.* **2014**, *43*, 7787 – 7812.
[18] S. Fukuzumi, Y. Yamada, *ChemSusChem* **2013**, *6*, 1834 – 1847.
[19] S. Fukuzumi, K. Ohkubo, *Dalton Trans.* **2013**, *42*, 15846 – 15858.
[20] T. Grewe, M. Meggouh, H. Tueysuez, *Chem. Asian J.* **2016**, *11*, 22 – 42.
[21] S. Fukuzumi, *Eur. J. Inorg. Chem.* **2008**, 1351 – 1362.
[22] X. Zou, Y. Zhang, *Chem. Soc. Rev.* **2015**, *44*, 5148 – 5180.
[23] S. Fukuzumi, *Bull. Chem. Soc. Jpn.* **2006**, *79*, 177 – 195.
[24] M. Suga, F. Akita, K. Hirata, G. Ueno, H. Murakami, Y. Nakajima, T. Shimizu, K. Yamashita, M. Yamamoto, H. Ago, J.-R. Shen, *Nature* **2015**, *517*, 99 – 103.
[25] Y. Umena, K. Kawakami, J.-R. Shen, N. Kamiya, *Nature* **2011**, *473*, 55 – 60.
[26] J. Yano, V. Yachandra, *Chem. Rev.* **2014**, *114*, 4175 – 4205.
[27] N. Cox, D. A. Pantazis, F. Neese, W. Lubitz, *Acc. Chem. Res.* **2013**, *46*, 1588 – 1596.
[28] M. D. Kärkäs, O. Verho, E. V. Johnston, B. Åkermark, *Chem. Rev.* **2014**, *114*, 11863 – 12001.
[29] L. Duan, L. Wang, F. Li, F. Li, L. Sun, *Acc. Chem. Res.* **2015**, *48*, 2084 – 2096.
[30] M. M. Najafpour, M. Z. Ghobadi, B. Haghighi, T. Tomo, J.-R. Shen, S. I. Allakhverdiev, *Biochim. Biophys. Acta Bioenerg.* **2015**, *1847*, 294 – 306.
[31] A. R. Parent, R. H. Crabtree, G. W. Brudvig, *Chem. Soc. Rev.* **2013**, *42*, 2247 – 2252.
[32] K. J. Young, B. J. Brennan, R. Tagore, G. W. Brudvig, *Acc. Chem. Res.* **2015**, *48*, 567 – 574.
[33] K. J. Young, L. A. Martini, R. L. Milot, R. C. Snoeberger, III, V. S. Batista, C. A. Schmuttenmaer, R. H. Crabtree, G. W. Brudvig, *Coord. Chem. Rev.* **2012**, *256*, 2503 – 2520.
[34] S. Fukuzumi, D. Hong, Y. Yamada, *J. Phys. Chem. Lett.* **2013**, *4*, 3458 – 3467.
[35] X. Wu, F. Li, B. Zhang, L. Sun, *J. Photochem. Photobiol. C* **2015**, *25*, 71 – 89.
[36] S. Fukuzumi, Y. Yamada, *J. Mater. Chem.* **2012**, *22*, 24284 – 24296.
[37] D. G. H. Hetterscheid, J. N. H. Reek, *Angew. Chem. Int. Ed.* **2012**, *51*, 9740 – 9747; *Angew. Chem.* **2012**, *124*, 9878 – 9885.
[38] D. J. Wasylenko, R. D. Palmer, C. P. Berlinguette, *Chem. Commun.* **2013**, *49*, 218 – 227.
[39] A. Sartorel, M. Bonchio, S. Campagna, F. Scandola, *Chem. Soc. Rev.* **2013**, *42*, 2262 – 2280.
[40] A. Lewandowska-Andralojc, D. E. Polyansky, *J. Phys. Chem. A* **2013**, *117*, 10311 – 10319.
[41] X. Du, Y. Ding, F. Song, B. Ma, J. Zhao, J. Song, *Chem. Commun.* **2015**, *51*, 13925 – 13928.
[42] F. Evangelisti, R. Moré, F. Hodel, S. Luber, G. R. Patzke, *J. Am. Chem. Soc.* **2015**, *137*, 11076 – 11084.
[43] F. Evangelisti, R. Güttinger, R. Moré, S. Luber, G. R. Patzke, *J. Am. Chem. Soc.* **2013**, *135*, 18734 – 18737.
[44] J. Wei, Y. Feng, P. Zhou, Y. Liu, J. Xu, R. Xiang, Y. Ding, C. Zhao, L. Fan, C. Hu, *ChemSusChem* **2015**, *8*, 2630 – 2634.
[45] Y. V. Geletii, Z. Huang, Y. Hou, D. G. Musaev, T. Lian, C. L. Hill, *J. Am. Chem. Soc.* **2009**, *131*, 7522 – 7523.
[46] X.-B. Han, Y.-G. Li, Z.-M. Zhang, H.-Q. Tan, Y. Lu, E.-B. Wang, *J. Am. Chem. Soc.* **2015**, *137*, 5486 – 5493.
[47] X.-B. Han, Z.-M. Zhang, T. Zhang, Y.-G. Li, W. Lin, W. You, Z.-M. Su, E.-B. Wang, *J. Am. Chem. Soc.* **2014**, *136*, 5359 – 5366.
[48] H. Lv, J. Song, Y. V. Geletii, J. W. Vickers, J. M. Sumliner, D. G. Musaev, P. Kögerler, P. F. Zhuk, J. Bacsa, G. Zhu, C. L. Hill, *J. Am. Chem. Soc.* **2014**, *136*, 9268 – 9271.
[49] T. Zhou, D. Wang, S. C.-K. Goh, J. Hong, J. Han, J. Mao, R. Xu, *Energy Environ. Sci.* **2015**, *8*, 526 – 534.
[50] R. Al-Oweini, A. Sartorel, B. S. Bassil, M. Natali, S. Berardi, F. Scandola, U. Kortz, M. Bonchio, *Angew. Chem. Int. Ed.* **2014**, *53*, 11182 – 11185; *Angew. Chem.* **2014**, *126*, 11364 – 11367.
[51] R. Xiang, Y. Ding, J. Zhao, *Chem. Asian J.* **2014**, *9*, 3228 – 3237.
[52] C. Besson, Z. Huang, Y. V. Geletii, S. Lense, K. I. Hardcastle, D. G. Musaev, T. Lian, A. Proust, C. L. Hill, *Chem. Commun.* **2010**, *46*, 2784 – 2786.
[53] S. Tanaka, M. Annaka, K. Sakai, *Chem. Commun.* **2012**, *48*, 1653 – 1655.
[54] B. Das, A. Orthaber, S. Ott, A. Thapper, *Chem. Commun.* **2015**, *51*, 13074 – 13077.
[55] M. Chen, S.-M. Ng, S.-M. Yiu, K.-C. Lau, R. J. Zeng, T.-C. Lau, *Chem. Commun.* **2014**, *50*, 14956 – 14959.
[56] T. Nakazono, A. R. Parent, K. Sakai, *Chem. Commun.* **2013**, *49*, 6325 – 6327.
[57] T. Nakazono, A. R. Parent, K. Sakai, *Chem. Eur. J.* **2015**, *21*, 6723 – 6726.
[58] C.-F. Leung, S.-M. Ng, C.-C. Ko, W.-L. Man, J. Wu, L. Chen, T.-C. Lau, *Energy Environ. Sci.* **2012**, *5*, 7903 – 7907.
[59] H. Li, F. Li, B. Zhang, X. Zhou, F. Yu, L. Sun, *J. Am. Chem. Soc.* **2015**, *137*, 4332 – 4335.
[60] L. Wang, L. Duan, L. Tong, L. Sun, *J. Catal.* **2013**, *306*, 129 – 132.
[61] L. Wang, M. Mirmohades, A. Brown, L. Duan, F. Li, Q. Daniel, R. Lomoth, L. Sun, L. Hammarström, *Inorg. Chem.* **2015**, *54*, 2742 – 2751.
[62] A. Lewandowska-Andralojc, D. E. Polyansky, R. Zong, R. P. Thummel, E. Fujita, *Phys. Chem. Chem. Phys.* **2013**, *15*, 14058 – 14068.
[63] C. Panda, J. Debgupta, D. D. Díaz, K. K. Singh, S. S. Gupta, B. B. Dhar, *J. Am. Chem. Soc.* **2014**, *136*, 12273 – 12282.
[64] M.-P. Santoni, G. L. Ganga, V. M. Nardo, M. Natali, F. Puntoriero, F. Scandola, S. Campagna, *J. Am. Chem. Soc.* **2014**, *136*, 8189 – 8192.
[65] S. Berardi, L. Francàs, S. Neudeck, S. Maji, J. Benet-Buchholz, F. Meyer, A. Llobet, *ChemSusChem* **2015**, *8*, 3688 – 3696.
[66] T. Ishizuka, A. Watanabe, H. Kotani, K. Satonaka, D. Hong, T. Wada, Y. Shiota, K. Yoshizawa, K. Ohara, K. Yamaguchi, S. Kato, S. Fukuzumi, T. Kojima, *Inorg. Chem.* **2016**, *55*, 1154 – 1164.
[67] Y. V. Geletii, B. Botar, P. Kögerler, D. A. Hillesheim, D. G. Musaev, C. L. Hill, *Angew. Chem. Int. Ed.* **2008**, *47*, 3896 – 3899; *Angew. Chem.* **2008**, *120*, 3960 – 3963.
[68] A. Sartorel, M. Carraro, G. Scorrano, R. D. Zorzi, S. Geremia, N. D. McDaniel, S. Bernhard, M. Bonchio, *J. Am. Chem. Soc.* **2008**, *130*, 5006 – 5007.
[69] Q. Yin, J. M. Tan, C. Besson, Y. V. Geletii, D. G. Musaev, A. E. Kuznetsov, Z. Luo, K. I. Hardcastle, C. L. Hill, *Science* **2010**, *328*, 342 – 345.
[70] S. Bang, Y.-M. Lee, S. Hong, K.-B. Cho, Y. Nishida, M. S. Seo, R. Sarangi, S. Fukuzumi, W. Nam, *Nat. Chem.* **2014**, *6*, 934 – 940.
[71] S. Fukuzumi, K. Ohkubo, Y.-M. Lee, W. Nam, *Chem. Eur. J.* **2015**, *21*, 17548 – 17559.
[72] M. Murakami, D. Hong, T. Suenobu, S. Fukuzumi, *J. Am. Chem. Soc.* **2011**, *133*, 11605 – 11613.
[73] D. K. Dogutan, R. McGuire, Jr., D. G. Nocera, *J. Am. Chem. Soc.* **2011**, *133*, 9178 – 9180.
[74] D. J. Wasylenko, R. D. Palmer, E. Schott, C. P. Berlinguette, *Chem. Commun.* **2012**, *48*, 2107 – 2109.
[75] D. Wang, J. T. Groves, *Proc. Natl. Acad. Sci. USA* **2013**, *110*, 15579 – 15584.
[76] L. Wang, L. Duan, Y. Wang, M. S. G. Ahlquist, L. Sun, *Chem. Commun.* **2014**, *50*, 12947 – 12950.
[77] S. Neudeck, S. Maji, I. López, S. Meyer, F. Meyer, A. Llobet, *J. Am. Chem. Soc.* **2014**, *136*, 24 – 27.
[78] F. Bozoglian, S. Romain, M. Z. Ertem, T. K. Todorova, C. Sens, J. Mola, M. Rodríguez, I. Romero, J. Benet-Buchholz, X. Fontrodona, C. J. Cramer, L. Gagliardi, A. Llobet, *J. Am. Chem. Soc.* **2009**, *131*, 15176 – 15187.
[79] X. Sala, S. Maji, R. Bofill, J. García-Antón, L. Escriche, A. Llobet, *Acc. Chem. Res.* **2014**, *47*, 504 – 516.
[80] D. Hong, M. Murakami, Y. Yamada, S. Fukuzumi, *Energy Environ. Sci.* **2012**, *5*, 5708 – 5716.
[81] S. Fukuzumi, D. Hong, *Eur. J. Inorg. Chem.* **2014**, 645 – 659.
[82] J. J. Stracke, R. G. Finke, *ACS Catal.* **2014**, *4*, 909 – 933.
[83] M. A. Asraf, H. A. Younus, M. Yusubov, F. Verpoort, *Catal. Sci. Technol.* **2015**, *5*, 4901 – 4925.
[84] J. J. Stracke, R. G. Finke, *ACS Catal.* **2014**, *4*, 79 – 89.
[85] J. J. Stracke, R. G. Finke, *ACS Catal.* **2013**, *3*, 1209 – 1219.
[86] S. Goberna-Ferrón, J. Soriano-López, J. R. Galán-Mascarós, M. Nyman, *Eur. J. Inorg. Chem.* **2015**, 2833 – 2840.

[87] S. Goberna-Ferrón, L. Vigara, J. Soriano-López, J. R. Galán-Mascarós, *Inorg. Chem.* **2012**, *51*, 11707 – 11715.
[88] J. Soriano-López, S. Goberna-Ferrón, L. Vigara, J. J. Carbó, J. M. Poblet, J. R. Galán-Mascarós, *Inorg. Chem.* **2013**, *52*, 4753 – 4755.
[89] J. W. Vickers, H. Lv, J. M. Sumliner, G. Zhu, Z. Luo, D. G. Musaev, Y. V. Geletii, C. L. Hill, *J. Am. Chem. Soc.* **2013**, *135*, 14110 – 14118.
[90] Y.-H. Lai, C.-Y. Lin, Y. Lv, T. C. King, A. Steiner, N. M. Muresan, L. Gan, D. S. Wright, E. Reisner, *Chem. Commun.* **2013**, *49*, 4331 – 4333.
[91] A. Savini, A. Bucci, G. Bellachioma, L. Rocchigiani, C. Zuccaccia, A. Llobet, A. Macchioni, *Eur. J. Inorg. Chem.* **2014**, 690 – 697.
[92] M. M. Najafpour, F. Ebrahimi, R. Safdari, M. Z. Ghobadi, M. Tavahodi, P. Rafighi, *Dalton Trans.* **2015**, *44*, 15435 – 15440.
[93] J. M. Thomsen, D. L. Huang, R. H. Crabtree, G. W. Brudvig, *Dalton Trans.* **2015**, *44*, 12452 – 12472.
[94] D. Hong, J. Jung, J. Park, Y. Yamada, T. Suenobu, Y.-M. Lee, W. Nam, S. Fukuzumi, *Energy Environ. Sci.* **2012**, *5*, 7606 – 7616.
[95] S. Fu, Y, Liu, Y. Ding, X. Du, F. Song, R. Xiang, B. Ma, *Chem. Commun.* **2014**, *50*, 2167 – 2169.
[96] H. Chen, Z. Sun, X. Liu, A. Han, P. Du, *J. Phys. Chem. C* **2015**, *119*, 8998 – 9004.
[97] G. Chen, L. Chen, S.-M. Ng, W.-L. Man, T.-C. Lau, *Angew. Chem. Int. Ed.* **2013**, *52*, 1789 – 1791; *Angew. Chem.* **2013**, *125*, 1833 – 1835.
[98] D. Hong, S. Mandal, Y. Yamada, Y.-M. Lee, W. Nam, A. Llobet, S. Fukuzumi, *Inorg. Chem.* **2013**, *52*, 9522 – 9531.
[99] H. Liu, M. Schilling, M. Yulikov, S. Luber, G. R. Patzke, *ACS Catal.* **2015**, *5*, 4994 – 4999.
[100] G. Chen, L. Chen, S.-M. Ng, T.-C. Lau, *ChemSusChem* **2014**, *7*, 127 – 134.
[101] A. Singh, S. L. Y. Chang, R. K. Hocking, U. Bach, L. Spiccia, *Energy Environ. Sci.* **2013**, *6*, 579 – 586.
[102] Y. Isaka, S. Kato, D. Hong, T. Suenobu, Y. Yamada, S. Fukuzumi, *J. Mater. Chem. A* **2015**, *3*, 12404 – 12412.
[103] S. Kato, J. Jung, T. Suenobu, S. Fukuzumi, *Energy Environ. Sci.* **2013**, *6*, 3756 – 3764.
[104] A. Harriman, I. J. Pickering, J. M. Thomas, *J. Chem. Soc. Faraday Trans. 1* **1988**, *84*, 2795 – 2806.
[105] A. Harriman, *Eur. J. Inorg. Chem.* **2014**, 573 – 580.
[106] M. Hara, C. C. Waraksa, J. T. Lean, B. A. Lewis, T. E. Mallouk, *J. Phys. Chem. A* **2000**, *104*, 5275 – 5280.
[107] M. Hara, J. T. Lean, T. E. Mallouk, *Chem. Mater.* **2001**, *13*, 4668 – 4675.
[108] F. A. Frame, T. K. Townsend, R. L. Chamousis, E. M. Sabio, T. Dittrich, N. D. Browning, F. E. Osterloh, *J. Am. Chem. Soc.* **2011**, *133*, 7264 – 7267.
[109] A. Harriman, M.-C. Richoux, P. A. Christensen, S. Mosseri, P. Neta, *J. Chem. Soc. Faraday Trans. 1* **1987**, *83*, 3001 – 3014.
[110] Y. Zhang, E. C. Judkins, D. R. McMillin, D. Mehta, T. Ren, *ACS Catal.* **2013**, *3*, 2474 – 2478.
[111] S. K. Das, P. K. Dutta, *Microporous Mesoporous Mater.* **1998**, *22*, 475 – 483.
[112] D. Hong, Y. Yamada, T. Nagatomi, Y. Takai, S. Fukuzumi, *J. Am. Chem. Soc.* **2012**, *134*, 19572 – 19575.
[113] X. Deng, H.-J. Bongard, C. K. Chan, H. Tüysüz, *ChemSusChem* **2015**, in press, DOI: 10.1002/cssc.201500872.
[114] X. Du, Y. Ding, C. Li, *ChemCatChem* **2015**, *7*, 2370 – 2376.
[115] Q. Xiang, G. Chen, T.-C. Lau, *RSC Adv.* **2015**, *5*, 52210 – 52216.
[116] X. Du, Y. Ding, R. Xiang, X. Xiang, *Phys. Chem. Chem. Phys.* **2015**, *17*, 10648 – 10655.
[117] Y. Yamada, K. Yano, D. Hong, S. Fukuzumi, *Phys. Chem. Chem. Phys.* **2012**, *14*, 5753 – 5760.
[118] D. Ressnig, M. Shalom, J. Patscheider, R. Moré, F. Evangelisti, M. Antonietta, G. R. Patzke, *J. Mater. Chem. A* **2015**, *3*, 5072 – 5082.
[119] D. Hong, Y. Yamada, A. Nomura, S. Fukuzumi, *Phys. Chem. Chem. Phys.* **2013**, *15*, 19125 – 19128.
[120] D. M. Robinson, Y. B. Go, M. Mui, G. Gardner, Z. Zhang, D. Mastrogiovanni, E. Garfunkel, J. Li, M. Greenblatt, G. C. Dismukes, *J. Am. Chem. Soc.* **2013**, *135*, 3494 – 3501.
[121] Y. Zhao, Y. Zhang, Y. Ding, M. Chen, *Dalton Trans.* **2015**, *44*, 15628 – 15635.
[122] T. Zhang, W. Lin, *Chem. Soc. Rev.* **2014**, *43*, 5982 – 5993.
[123] S. Pintado, S. Goberna-Ferron, E. C. Escudero-Adan, J. R. Galan-Mascarós, *J. Am. Chem. Soc.* **2013**, *135*, 13270 – 13273.
[124] X.-P. Shen, Y.-Z. Li, Y. Song, Z. Xu, G.-C. Guo, *Eur. J. Inorg. Chem.* **2007**, 1698 – 1702.
[125] Y. Yamada, K. Oyama, R. Gates, S. Fukuzumi, *Angew. Chem. Int. Ed.* **2015**, *54*, 5613 – 5617; *Angew. Chem.* **2015**, *127*, 5705 – 5709.
[126] R. D. Shannon, *Acta Crystallogr. Sect. A* **1976**, *32*, 751 – 767.

Manuscript received: November 30, 2015
Final Article published: February 17, 2016